

A.E. Armstrong · L.-B. Tremblay · L.A. Mysak

A data-model intercomparison study of Arctic sea-ice variability

Received: 14 May 2002 / Accepted: 15 August 2002 / Published online: 14 January 2003
© Springer-Verlag 2003

Abstract The dynamic-thermodynamic granular rheology sea-ice model of Tremblay and Mysak is validated against 40 years of observed sea-ice concentration (SIC) data. Subsequently, the mechanisms responsible for producing SIC anomalies in the model are evaluated by studying the coupled variance (using the singular value decomposition method, SVD) between the simulated SIC anomalies and the ice speed and air temperature anomalies. To execute this validation, a 49-year (1949–97) simulation (including a 9-year spin-up period) of the Arctic and peripheral sea-ice cover using daily varying winds and monthly mean air temperatures is produced. In general, the simulated SIC variations for 1958–97 in the East Siberian, Chukchi and Beaufort seas are in agreement with observations, while larger discrepancies occur in the Laptev and Kara seas. Moreover, the sensitivity of the model to southerly wind anomalies in creating summer SIC anomalies compares well with the observed sensitivity; however, the model's sensitivity to summer air temperature anomalies is weaker than observed. The summer SIC anomalies over an entire sea are not influenced by variations in the level of river runoff. Results from the SVD analysis show that the main source of variability in the peripheral seas is associated with the variation in the strength of the Arctic High; in the East Siberian and Laptev seas, the strengthening and weakening of the Transpolar Drift Stream also play an important role. Over the entire Arctic domain, surface air temperature anomalies are negatively correlated with sea-ice anomalies. Finally, the observed downward trend in total sea-ice cover in the

last two decades as well as record minima in the East Siberian Sea are well reproduced in the simulation.

1 Introduction

The Arctic Ocean sea-ice cover varies annually in its areal extent from a minimum of 7.8×10^6 km² in September to 14.8×10^6 km² in March (Barry et al. 1993), with maximum interannual variations of up to 0.5×10^6 km² (Cavalieri et al. 1997). Superimposed on this interannual variability is a downward trend in the areal extent of the Arctic Ocean sea-ice cover in the last two decades (Cavalieri et al. 1997; Parkinson et al. 1999), which is mainly apparent during the summer months. Such variations in summer SICs will have an influence on high-latitude climate in a number of ways. A smaller ice extent will, for example, lead to an increased absorption of shortwave radiation by the relatively darker ocean surface in peripheral seas and possibly, to a further decrease in sea-ice cover. It will also lead to an increase in the mixing of river runoff with shelf water. These two effects will have an influence on the stratification and the heat content of the mixed-layer and hence on the timing of the next fall freeze-up. Also, biological productivity which relies heavily on the presence of light and the release of nutrients by the melting sea ice will follow closely the changing ice-edge position. Finally, fluctuations in summer sea-ice cover will affect the navigability in the peripheral seas of the Arctic Ocean.

Relative minima and decreases in Arctic sea-ice cover have recently been observed and analyzed by Chapman and Walsh (1993), Maslanik et al. (1996), Cavalieri et al. (1997) and Parkinson et al. (1999). Maslanik et al. (1996) studied Arctic summer ice concentration and extent and reported ice concentrations in September 1993 to be at a 17-year low. They also reported that some areas consistently covered by ice from 1979 to 1989 were ice-free in 1990, 1993 and 1995. Cavalieri et al. (1997) analyzed passive microwave satellite observations and found that

A.E. Armstrong (✉) · L.A. Mysak
Department of Atmospheric and Oceanic Sciences and Centre
for Climate and Global Change Research, McGill University,
805 Sherbrooke Street West, Montreal, Quebec, Canada, H3A 2K6
E-mail: anne.armstrong@mail.mcgill.ca

L.-B. Tremblay
Lamont-Doherty Earth Observatory of Columbia University,
Rt. 9W, Palisades, NY U.S.A. 10964-8000

from November 1978 through December 1996, the areal extent of sea ice decreased by $2.9 \pm 0.4\%$ per decade in the Arctic. Parkinson et al. (1999) calculated an overall decreasing trend of 2.8% per decade in Arctic sea-ice extents (through a regional analysis of observational data) over the same 18-year period. Chapman and Walsh (1993) reported similar trends and also that new summer relative minima had been achieved three times in the years 1976–1990; however, they found no apparent decreases for the Arctic sea-ice extent for winter.

Data analysis studies of the sea-ice cover generally demonstrate that its interannual variability tends to be organized into geographical patterns that are closely related to dominant structures of atmospheric circulation variability patterns (Slonosky et al. 1997; Mysak and Venegas 1998; Deser et al. 2000), which locally manifest themselves as surface air temperature and wind anomalies (Prinsenberg et al. 1997). One objective of this study is to determine how well the temporal and spatial patterns of sea-ice cover variability in the Arctic Ocean and peripheral seas can be reproduced by the thermodynamic-dynamic model of Tremblay and Mysak (1997). In particular, the ability of the model to simulate the year-to-year variability in sea-ice cover and extreme events in the diminution of its areal extent is examined. This study complements the work of Arfeuille et al. (2000) which focused on analyzing the variability of the sea-ice volume in the Arctic Ocean. To achieve this objective, a 40-year simulation of the Arctic sea-ice cover and peripheral seas is compared with observed sea-ice concentration (SIC) data obtained from the Hadley Centre for Meteorological Research (HadISST data set). A second purpose is to examine the relative importance of dynamic and thermodynamic effects on the SIC variability within the Arctic region, by studying the response of simulated and observed SIC to air temperature and wind forcing anomalies from the NCEP (National Centers for Environmental Prediction) reanalysis project, and the co-variability of the simulated fields using the singular value decomposition (SVD) method of analysis. By-products of this study are the validation of NCEP surface air temperatures against station data and the determination of the role river runoff plays in producing summer SIC anomalies.

A brief description of the coupled slab ocean sea-ice model employed is given in Sect. 2. The HadISST data set used in this study is described in Sect. 3. In Sect. 4, a discussion of the data-model intercomparison is presented. The main conclusions drawn from this investigation are summarized in Sect. 5.

2 Sea-ice model

In the model of Tremblay and Mysak (1997) the sea-ice cover is considered to consist of many floes and is assumed to behave as a large-scale granular material in slow continuous deformation under the action of the winds and ocean currents. The resistance of sea ice to a compressive load is considered to be a function of its thickness and concentration, and its shear resistance is proportional to the

internal ice pressure at a point. In divergent motion, the ice offers no resistance and the floes drift freely. The boundary conditions for the ice dynamic equations are zero normal and tangential velocity at a solid boundary and free outflow at open boundaries (Hibler 1979). Thermodynamically, a simple two-category (ice and no ice) model is used, which calculates the mean ice thickness and concentration in a grid cell (Hibler 1979). In the vertical, the zero-layer model of Semtner (1976) with a linear temperature profile from the ice base to the ice surface is used. This type of model is appropriate for ice thicknesses smaller than about 3 m when using monthly averaged atmospheric forcing.

The sea-ice model is coupled thermodynamically to a slab ocean with prescribed steady, but spatially varying ocean currents. At open boundaries (Bering Strait, Greenland/Norwegian seas) the temperatures are specified from monthly climatologies extracted from Levitus (1994); at continental boundaries, the horizontal ocean heat flux is set to zero. In this model, the ocean is allowed to warm up despite the presence of ice in a grid cell. The transfer of heat between the ocean and the ice is achieved through sensible heat transfer, in a similar manner to the heat transfer between the ice and the atmosphere. This gives a more realistic ice retreat during the melt season. A more complete description of this model can be found in Tremblay and Mysak (1997).

3 HadISST data set

The UK Hadley Centre Global Ice and Sea Surface Temperature data set (HadISST) used in this study contains monthly mean sea surface temperature (SST) and sea-ice coverage data from 1871 to the present. In the following analyses, end-of-month Arctic SIC data from HadISST on a 1° latitude by 1° longitude grid for the period of 1958 to 1997 are used. The SIC for these years of study in HadISST are a merging of several data sets, including the Walsh Northern Hemisphere SIC charts (Walsh 1995), the National Ice Center charts and passive microwave retrievals [from the Scanning Multichannel Microwave Radiometer (SSMR) and Special Sensor Microwave/Imager (SSM/I) instruments carried on Nimbus 7 and the Defense Meteorological Satellite Program].

Prior to 1972, the SIC data are less homogeneous than those of the satellite era due to (1) changes in the analysis procedures used by several agencies (Chapman and Walsh 1993) which results in inconsistencies in overlapping data (Walsh 1978); (2) the use of “estimated” concentrations in some analyses; and (3) the need to temporally interpolate data for some regions when no data were available for a particular month (Chapman and Walsh 1993). As well, the Walsh data set prior to 1979 contains large areas having 100% SIC, and thus lacks a realistic spatial variability which would be more consistent with the leads and other fractures present in the ice. The satellite-derived SIC can be overestimated by up to 10% when liquid water cloud is present (Oelke 1996); the overestimation depends on surface type: open ocean, first-year ice or multi-year ice. In contrast, melt-ponds resting atop the ice cover yield lower SIC than observed. The “penetration depth” of liquid water at microwave frequencies is very shallow and so even a thin layer of water on top of the ice could yield the same low emissivities as would be seen for a calm open ocean. Thus melt-ponds result in an underestimation of the amount of SIC. Finally, the liquid water within the snow pack when melting first begins leads to an increased emissivity at passive microwave frequencies and therefore an overestimation of SIC (J.A. Maslanik personal communication 2000). The HadISST data set has been massaged in order to try to alleviate some of the above mentioned problems. This massaging includes “correcting” the summer melt bias in the passive microwave retrievals due to surface melt and ponding, and by adding spatial variability to the Walsh SIC data. A complete description of this data set including the sources and merging procedure can be found in Rayner et al. (in press 2002).

To ease comparison between model results and observations, the HadISST data were bi-linearly interpolated onto the model cartesian grid (110 km \times 110 km resolution), which includes the

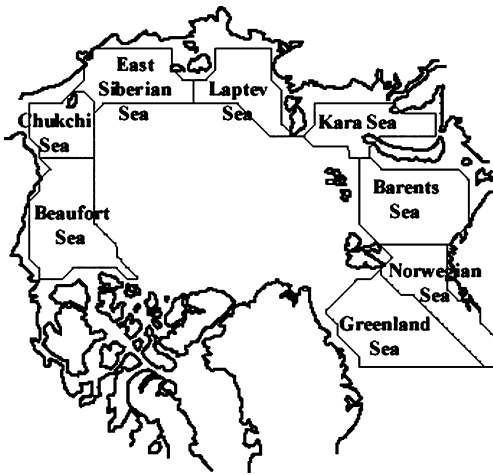


Fig. 1 Map of the Arctic and peripheral seas, as defined for this study

Arctic, its peripheral seas and the Nordic seas (Greenland-Iceland-Norwegian seas, see Fig. 1). First, the HadISST data set was scanned for patches of missing data. For the grid cells bordering these regions of missing data (where the model grid cell was sometimes not surrounded by all four grid cells of SIC observational data), the SIC was extrapolated linearly. For grid cells interior to these regions, no attempt was made to “create” information and the region was flagged as missing data.

4 Results

In this section, the last 40 years of simulated SIC anomalies from a 49-year run (1949–97) using the Tremblay and Mysak (1997) sea-ice model are presented. In this run, the first nine years (1949–57) are used to spin-up the model and are not included in the model-data intercomparison analysis. The model is forced with daily varying winds and monthly mean varying air temperatures and humidity derived from the NCEP re-analysis data. The model physical domain includes the Arctic Ocean and the Nordic seas (see Fig. 1).

Simulated and observed time series of monthly SIC anomalies are first compared for each of the Arctic Ocean’s peripheral seas and Nordic seas. In an attempt to better understand the differences between the simulated and observed SIC anomalies, the NCEP air temperatures used to force the model are compared with measured air temperatures at various Arctic coastal stations from the Environmental Working Group Joint US-Russian Arctic atlas. Next, the potential effects of river runoff on summer SIC anomalies are investigated from observed SIC and river runoff data. This is followed by a study of the model SIC sensitivity to dynamic (wind) and thermodynamic (air temperature) forcing during summer.

Singular value decomposition (SVD) analysis of simulated SIC and sea-ice drift speeds, as well as simulated SIC and atmospheric temperature is then used to determine the links between sea-ice dynamic/thermodynamic effects and SIC anomalies and their relative importance in creating sea-ice anomalies in the Arctic.

In the SVD analysis, the sea-ice drift speed is used as a proxy for wind. This approach allows for a more direct assessment of the link between sea-ice motion and the mechanisms responsible for the formation of SIC anomalies. As well, it is indicative of its link with wind forcing, as sea-ice drifts mostly follow isobars except in certain regions where ice floe interaction is very small or very large (see for instance, passive microwave derived sea-ice velocity from Kwok, http://www.radar.jpl.nasa.gov/rgps/image_files/930408_grid.gif). The ratio of ice drift speed to surface wind speed can vary substantially, particularly when ice is thick and compact over a large area. Since this could be a limiting factor in analyzing the SVD results of the coupled SIC anomalies and SLP anomalies, SVD analysis was used to examine the coupled variance between the simulated SIC anomalies and SLP anomalies. The spatial patterns of the first mode were a smoother version of the coupled SIC anomalies and sea-ice speed anomalies shown in Fig. 5 and therefore are not presented here. Yi et al. (1999) presented an SVD analysis of SIC and sea level pressure (SLP) for the region poleward of 45°N; however, on this scale, the co-variability is dominated by an NAO-like SLP pattern and the Greenland/Barents – Labrador seas SIC dipole. Finally, the simulated sea-ice extent anomalies for the total Arctic for 1958–97 are shown and compared with the recent (1978–96) observed trend in the sea anomalies.

4.1 Regional time series

For each region shown in Fig. 1, anomalies of spatially averaged monthly mean SIC were calculated, for both simulated and observed data (Fig. 2). The correlation coefficients between the modelled and observed time series were then calculated to assess the level of the agreement. In the following, the 95% significance level (estimated using a two sided *t*-test) is presented in square brackets following the correlation coefficient with which it is associated. In general, the simulated and observed SIC anomalies are in agreement for the Beaufort, Chukchi, East Siberian and Laptev seas (Fig. 2a–d) and less so for the Kara Sea (Fig. 2e). A striking feature common to several of the peripheral seas is the large negative anomalies observed in the 1990s (especially apparent in the Chukchi and East Siberian seas). The Arctic Oscillation (AO) index was very positive in the 1990s (Thompson and Wallace 1998) causing negative SIC anomalies in the Laptev and East Siberian seas (a correlation map, not presented, between the observed anomalous SIC and the NAO index shows negative centres of action in both the Laptev and East Siberian seas). Some of these negative SIC anomalies are reproduced by the model (see Fig. 2b, c). The presence of melt ponds, which are interpreted as open water by the passive microwave retrievals, is also believed to be partially responsible for the observed low SIC (N. Rayner personal communication 2001). Ignoring the change in

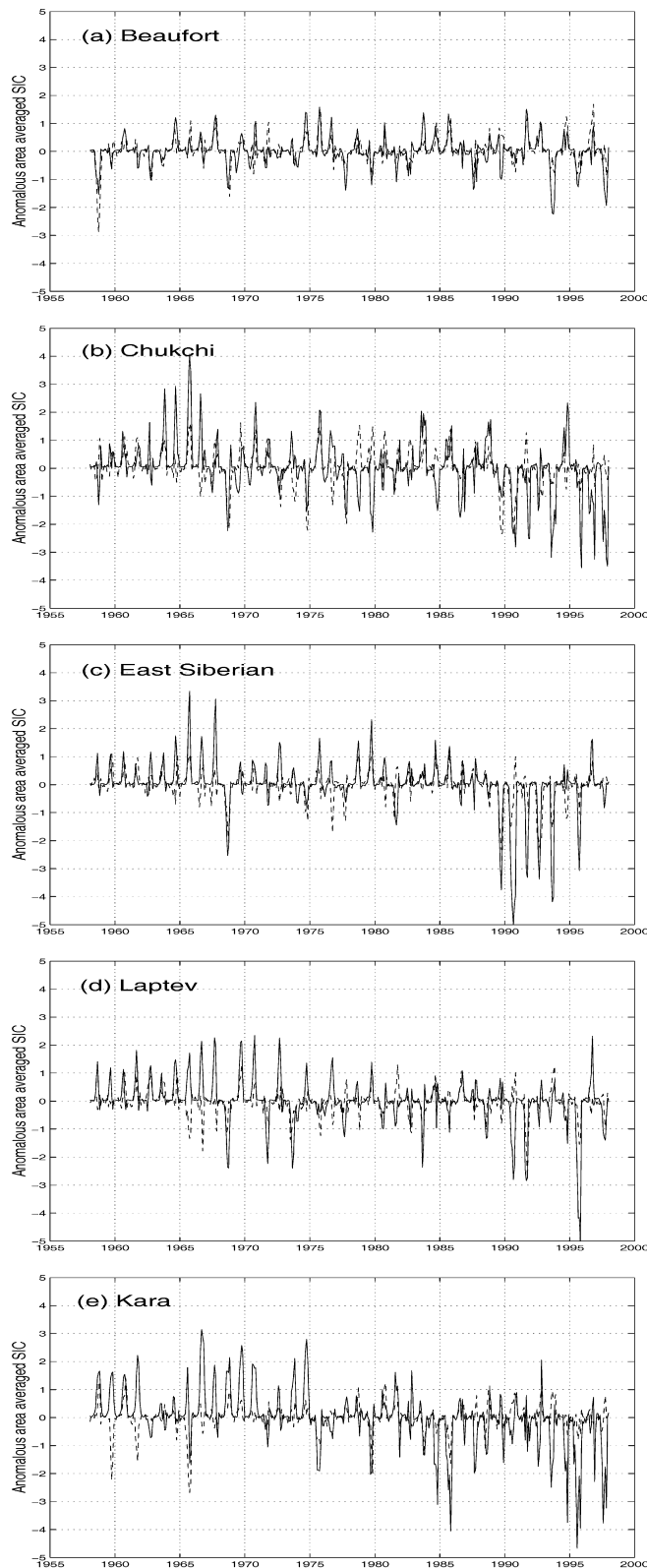


Fig. 2 Time series of observed (*solid*) and modelled (*dashed*) area averaged anomalous SIC (expressed in tenths) for the **a** Beaufort, **b** Chukchi, **c** East Siberian, **d** Laptev and **e** Kara seas. The correlation coefficients between the two time series in each plot are 0.67 [0.13], 0.41 [0.13], 0.54 [0.13], 0.41 [0.13] and 0.24 [0.13]

the mean SIC value in the 1990s as compared to the earlier part of the data set, the relative observed year-to-year changes in SIC seem to be captured by the model.

In the Chukchi Sea (Fig. 2b), the agreement between the two time series is lower than in its two adjacent seas (Beaufort and East Siberian seas): a possible reason for this is the omission of the interannually varying Bering Strait inflow in this region (Coachman and Aagaard 1988). Extreme minima in the 1990s, unprecedented within the passive microwave SIC record and primarily reflecting reduced ice cover over the East Siberian and Laptev Seas (Maslanik et al. 1996; Serreze et al. 1995), are also apparent in the time series of the modelled SIC (see Fig. 2c, d).

The spatially averaged time series of SIC in the Greenland, Norwegian and Barents Seas (not shown) yield lower correlations between the observed and simulated data of 0.23 [0.13], 0.21 [0.13] and 0.22 [0.13] respectively. These lower correlations suggest that other key processes and features absent in the present model may also be important for determining the SIC variability in the Greenland, Norwegian and Barents seas. For example, the temporal variability of the North Atlantic Drift inflow (prescribed as constant in the model) strongly influences the sea-ice cover in the Norwegian and Barents seas (Dickson et al. 2000). Further, the mixed layer depth (held fixed everywhere in the model) and ocean stratification differ greatly in the Arctic and the Greenland Sea (Zhang et al. 1998). In particular, because of the relatively weak stratification in the Greenland Sea, winter convective overturn can bring large quantities of heat into the upper ocean which melts the sea ice there (Broecker and Denton 1990).

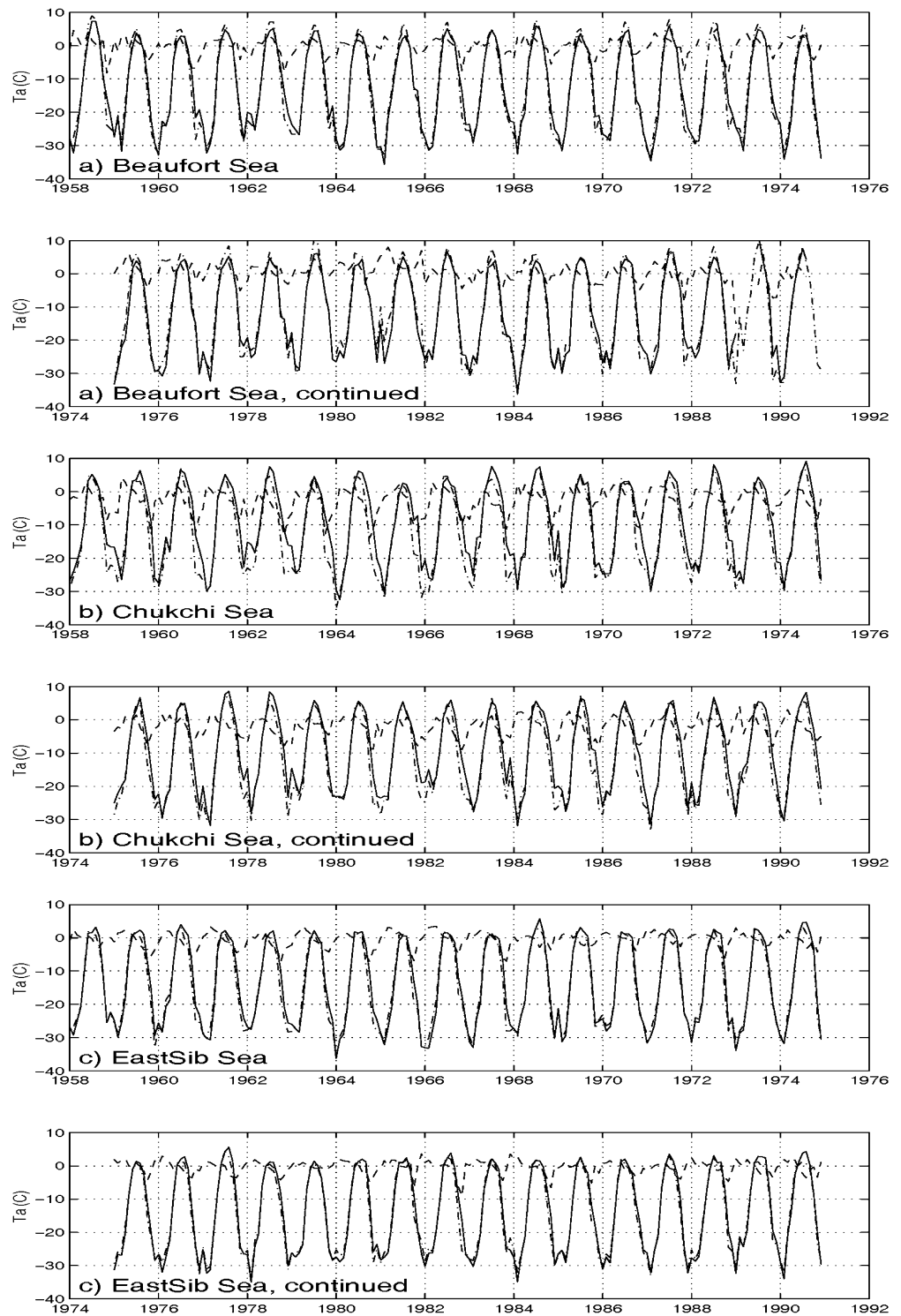
4.2 Assessment of the NCEP thermodynamic forcing

In order to better understand the discrepancies between the observed and simulated SIC anomalies in the peripheral seas of the Arctic presented above, a number of factors were analyzed. First the NCEP air temperatures used to force the model were compared with coastal station air temperatures taken from the Environmental Working Group (EWG) Joint US-Russian Arctic Atlas as a means of verifying the quality of the thermodynamic forcings of the model. Time series for one station in each of the peripheral seas are shown in Fig. 3.

In general, the NCEP temperatures are in good agreement with measured surface air temperature from the EWG working group, although some discrepancies do exist. Nevertheless, correlations between summer mean air temperature errors (NCEP minus EWG air temperatures) and SIC anomaly errors (simulated minus observed SIC anomalies) are statistically insignificant, and thus these temperature differences are not likely a major factor in the discrepancies found between simulated and observed SIC anomalies.

In fall, the NCEP air temperatures systematically lead the station (coastal) values by 15 days. The fall lead

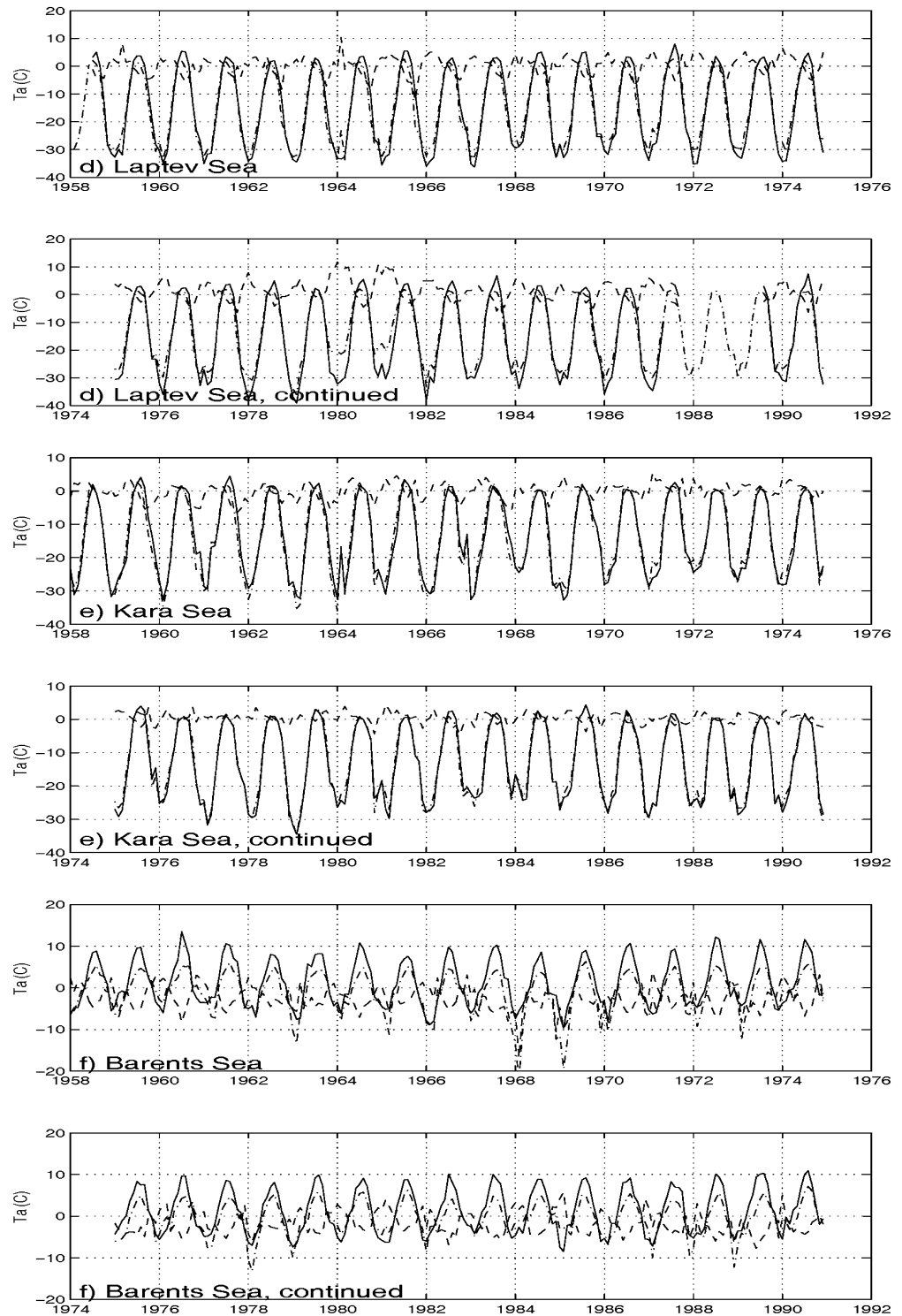
Fig. 3 Time series of measured (solid line) and NCEP (dashed dot) surface air temperature in the **a** Beaufort, **b** Chukchi, **c** East Siberian, **d** Laptev, **e** Kara and **f** Barents seas. The measured EWG data used is from Barter Island (WMO Station 70086, 70.10N 216.40E) for the Beaufort Sea, Ostrov Koluchin (WMO Station 25286, 67.47N 185.37E) for the Chukchi Sea, Ostrov Chetyrehstolbovoy (WMO Station 21965, 70.63N 162.40E) for East Siberian Sea, Ostrov Dunay (WMO Station 21613, 73.93N 124.50E) for the Laptev Sea, Ostrov Izvestig Zik (WMO Station 20471, 75.92N 83.08E) for the Kara Sea and Vardo (WMO station 81098, 70.40N 31.10E) for the Barents Sea. The difference between NCEP and measured air temperature at each station is shown as a dashed line



in the NCEP air temperature data is due to the way the surface boundary condition in the NCEP reanalysis is specified. In the NCEP reanalysis simulations, the surface conditions (i.e., ice concentration) in ice covered seas are taken from the GISTT data set. In order to calculate the surface temperature and the ocean-atmosphere heat flux, the ice thickness is also required. NCEP assumes a 3 m ice thickness with no lead fraction as soon as the ice is present in the fall (Markia Holland

personal communication 2002; Bitz et al. 2002). Since the ice thickness in the peripheral seas is about 1 m in late winter and much thinner in the fall this would limit the heat fluxes from the ocean to the atmosphere resulting in a colder overlying air temperature. However, this time-lead would have more of an effect on the timing of the seasonal cycle. In the Beaufort Sea (Fig. 3a), there is a systematic temperature bias of approximately two degrees in the summer, with

Fig. 3 (Contd.)



NCEP temperatures being warmer. Such a temperature difference in summer can lead to a significantly different surface energy budget and consequently a very different total summer melt (Flato and Brown 1996). This could have an effect on the long term and interannual variability of the sea-ice cover. As will be seen later, the sensitivity of the model to thermodynamic forcing is lower than in reality, and a good correspondence be-

tween observed and simulated SIC was still possible. In the Chukchi Sea (Fig. 3b), some discrepancies exist in the December, January air temperatures with NCEP temperatures often being colder. The most striking feature, however, occurs in the Laptev Sea (Fig. 3d) for the winters 1980 and 1981 with peak winter temperatures being ten degrees warmer than observed. A five degree discrepancy of the NCEP temperatures for the winters of

1976, 1978 and 1987 is also noted. As well, the NCEP temperatures seem to be colder by approximately two degrees in the peak summer months. Again, this could lead to differences in the simulated SIC variability. In the Barents Sea (Fig. 3f), differences in air temperature of three to four degrees in both winter and summer are also present, with NCEP temperatures being colder than station data. In the East Siberian and Kara Seas, the agreement between observed and NCEP temperatures is very good.

4.3 Sensitivity of summer SIC anomalies to river runoff and summer southerly wind and air temperature anomalies

The monthly mean river runoff anomalies for each peripheral sea are shown in Fig. 4 along with the corresponding regional observed summer SIC anomalies. The goal is to determine whether positive anomalies in river runoff could lead to an earlier ice cover breakup and negative summer SIC anomalies due to the ice-albedo feedback. The simulated SIC anomalies are not shown as the vertical resolution in the slab ocean model is too coarse to resolve the effects of river runoff. The river runoff data presented in Fig. 4 were compiled by Newton (2001) from various sources, including Becker (1995), Roach et al. (1995), Atmospheric Environment Service (1994) and C. Bromwich (personal communication 1996). The correlation coefficients for the time series (Fig. 4) in each sea are not significant: i.e. the level of river runoff does not seem to affect the summer SICs of any particular entire sea. However, in an EOF analysis of SIC in the Beaufort Sea, Chouinard and Garrigues (1995) did find a local effect of the river runoff decreasing sea ice conditions near the river mouth, thereby forcing the spring break-up to come earlier.

In order to assess the model's sensitivity to thermodynamic and dynamic effects and to compare it to the observed sensitivity, monthly mean southerly wind and air temperature time series for each peripheral sea were compiled from the NCEP data set. The two time series were then correlated with the model and observed SIC anomaly time series for each peripheral sea. For the southerly wind and air temperature anomalies, early summer (May–July) and summer (June–August) averages were used respectively. For the SIC anomalies, late summer (July–September) averages were used. The averaging period for these indices takes into account the advective and thermodynamic time scales associated with the formation of sea ice anomalies, as a lag between wind (or air temperatures) and the formation of SIC anomalies is expected (Tremblay and Mysak 1998). These correlations are presented in Table 1. The averaging period for the two indices takes into account the advective and thermodynamic time scales associated with the formation of sea-ice anomalies (Tremblay and Mysak 1998). The correlation coefficients for the ob-

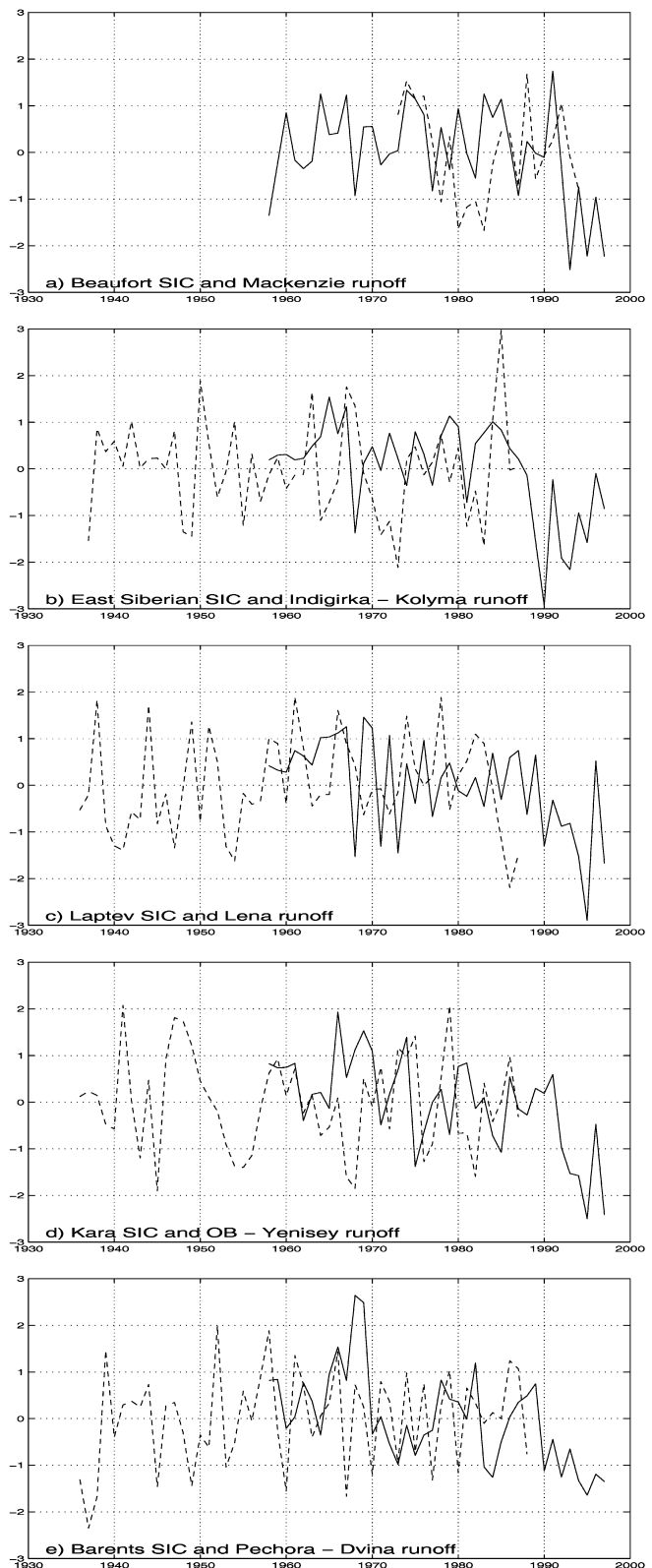


Fig. 4 Time series of normalized observed summer SIC anomalies (solid line) and river runoff (dashed line) for the **a** Beaufort, **b** East Siberian, **c** Laptev, **d** Kara and **e** Barents seas. The river runoff time series comprise the **a** MacKenzie, **b** the Indigirka and Kolyma, **c** Lena, **d** Ob and Yenisey and, **e** the Pechora and Dvina rivers

served SIC time series show that the thermodynamic effects dominate over dynamic effects in producing SIC anomalies, especially in the East Siberian, Laptev, Kara and Barents seas where thinner ice is present. Also, the model's sensitivity to dynamic effects is in very good agreement with the observed sensitivity. The model does not, however, seem to be sensitive enough to thermodynamic forcing. This is especially true in the East Siberian and Laptev seas where thicker ice is present in the mean simulated climate, reducing the sensitivity of

the model to thermodynamic forcing. It should be mentioned that control experiments were performed in order to isolate the effects of the two types of forcing. The model simulation was repeated using, (1) climatological winds and monthly varying temperatures and (2) climatological temperatures and daily varying winds. The simulated results using climatological temperatures were not significantly different from the run presented here, confirming again that the model is not sensitive enough to thermodynamic forcing.

Table 1 Correlation coefficients between early summer (May–July) southerly wind anomalies (Va) and late summer (July–September) SIC anomalies for each peripheral sea (first two columns) for both simulated and observed data. The last two columns contain the correlation coefficients between summer (June–August) air temperature anomalies (Ta) and late summer (July–September) SIC anomalies for each peripheral sea. The last correlation in the last column is not statistically significant at the 95% level

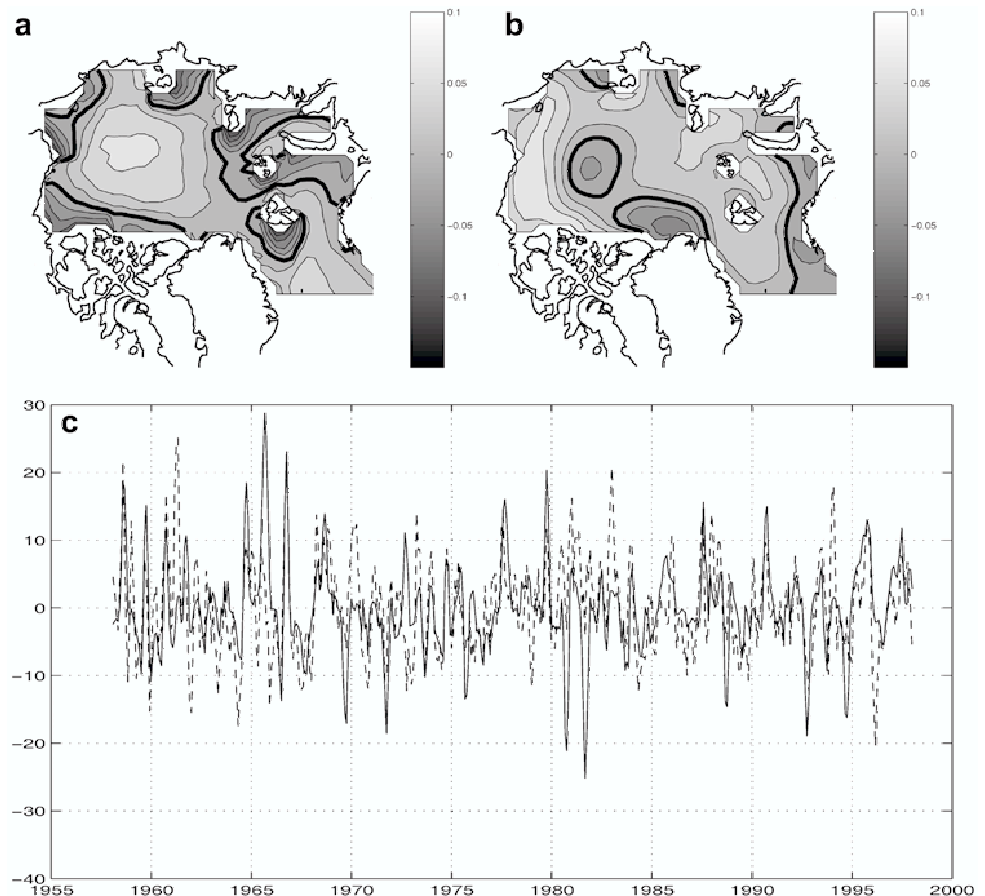
Sea	Va		Ta	
	Observed	Simulated	Observed	Simulated
Beaufort	0.50	0.47	0.65	0.58
Chukchi	0.66	0.67	0.82	0.50
East Siberian	0.34	0.42	0.69	0.46
Laptev	0.40	0.54	0.68	0.40
Kara	0.15	0.60	0.60	0.50
Barents	0.30	0.30	0.60	[0.26]

4.4 SVD analysis

The spatial and temporal patterns of sea-ice variability were next studied using the SVD method of analysis in order to identify pairs of coupled spatial patterns for (1) simulated SIC and sea-ice speed anomalies, and (2) simulated SIC and air temperature anomalies.

The leading SVD mode of the coupled SIC anomalies and sea-ice speed anomalies during the period 1958–97, which accounts for 41% of the total square covariance, is shown in Fig. 5. The correlation coefficient between the expansion coefficients of the coupled fields is 0.47 [0.13]. The largest positive SIC anomalies are found in the centre of the Beaufort Gyre (Fig. 5a), whereas away from the centre of the Gyre, the anomalies decrease in magnitude, becoming negative in the peripheral seas.

Fig. 5 Leading SVD mode of the **a** coupled sea-ice concentration (SIC) anomalies and **b** sea-ice speed anomalies during 1958–97. The contour interval is 0.02 and the *darkened line* is the zero contour. The square covariance fraction corresponding to this mode is 41%. The *solid* and *dashed* lines in **c** represent the three-month-running mean of the time series of the expansion coefficients for the coupled SIC and sea-ice speed anomalies respectively. The correlation coefficient between the expansion coefficients of both variables is 0.47 [0.13]



Similarly, low ice speeds are present at the centre of the Gyre (Fig. 5b), and higher speeds occur away from the centre of the Gyre. On average, the sea-ice drift circulation in the central-western Arctic is clockwise (the Beaufort Gyre) due to the climatological Arctic High pressure system in the winter which dominates the yearly average. This results in low level divergence in the atmosphere and surface convergence in the ocean. Any strengthening (weakening) of the Arctic High will cause an increased convergence (divergence) at the centre of the High and a lower sea-ice drift speed there due to increased (decreased) interactions, as seen in Fig. 5a, b. Conversely, larger ice speed and negative SIC anomalies will be present in the peripheral seas. The fact that this first mode accounts for 41% of the covariance along with the high correlation between the expansion coefficients suggest that SIC in the central Arctic, as governed by wind speed, reacts first to changes in surface convergence and divergence associated with the strength of the Arctic High.

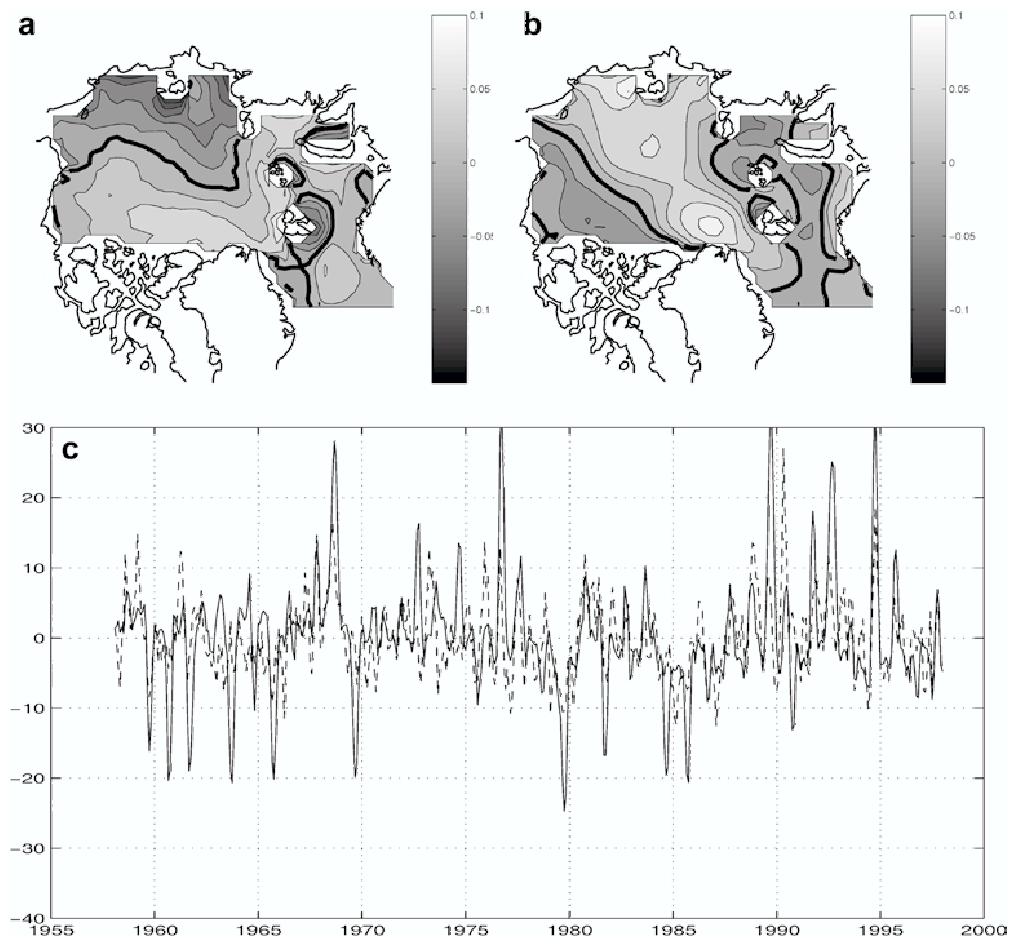
The second SVD mode of the coupled SIC anomalies and sea-ice speed anomalies during the period 1958–97, which accounts for 23% of the total square covariance, is shown in Fig. 6. The largest negative SIC anomalies are present in the East Siberian Sea (Fig. 6a), with a tongue extending out toward Fram

Strait that is accompanied by a positive ice speed anomaly (Fig. 6b). This tongue is associated with the Transpolar Drift Stream, which exports ice from the eastern Arctic through Fram Strait, into the Greenland Sea. Hence, any positive (negative) fluctuations in the strength of the Transpolar Drift Stream will cause negative (positive) anomalies in the SIC in the East Siberian Sea and in the tongue which extends out toward Fram Strait. For instance, in 1968, a year with a particularly broad Transpolar Drift Stream exporting ice out of the Laptev Sea. A strong signal in both the SIC and sea-ice speed expansion coefficients (Fig. 6c) is evident.

Finally, the geostrophic winds in the Kara and Laptev seas, on average, tend to push ice out of these regions, and so an increase in the wind speed results in an increase in ice export out of both the Kara and Laptev seas. This is apparent in Fig. 6 with negative ice anomalies and positive ice speed anomalies present in these seas. Given that the correlation coefficient between the expansion coefficients of the two variables is moderately high, it is seen that anomalous wind speeds play an important role in determining ice concentrations in the East Siberian Sea at the base of the Transpolar Drift Stream.

The correlation coefficient between the expansion coefficients of the SIC anomalies and sea-ice speed

Fig. 6 Second SVD mode of **a** the coupled sea-ice concentration (SIC) anomalies and **b** sea-ice speed anomalies during 1958–97. The contour interval is 0.02 and the *darkened line* is the zero contour. The square covariance fraction corresponding to this mode is 23%. The *solid* and *dashed* lines in **c** represent the three-month-running mean of the time series of the expansion coefficients for the coupled SIC and sea-ice speed anomalies respectively. The correlation coefficient between the expansion coefficients of both variables is 0.43 [0.13]



anomalies for the third SVD (not shown), which accounts for 12% of the total square covariance, is 0.50 [0.13]. The physical interpretation of these spatial patterns is that anomalously low winds in the Fram Strait area result in less ice than normal being advected out of the Arctic and hence negative anomalies of SIC in the Greenland Sea (or vice versa).

The leading SVD mode of the coupled SIC anomalies and surface air temperature anomalies during the period 1958–97, which accounts for 57% of the total square covariance, is shown in Fig. 7. The dipole structure in the air temperature field of this coupled mode is accompanied by an opposite dipole structure in the SIC field, as expected since higher air temperatures will lead to lower SIC. The correlation coefficient between the expansion coefficients of both variables is 0.46. The second and third SVD coupled modes for SIC and air temperature anomalies are not shown as they are effectively degenerate modes, according to the criterion of North et al. (1982).

4.5 Time series of the extent of Arctic sea-ice cover

The time series of the total simulated sea-ice cover area (with SIC greater than 15%) for the central Arctic and

its peripheral seas (excluding the Greenland, Norwegian, Barents and Kara seas), is presented in Fig. 8. Also included is a linear trend line that best fits the simulated time series data (in a least-squares sense) for the November 1978 to December 1996 time period (following Cavalieri et al. 1997; Parkinson et al. 1999). The trend from the simulated results is -1.1% per decade as compared to the observed trend of -2.9% reported in Cavalieri et al. (1997). The low sensitivity of the model to the thermodynamic forcing could be partly responsible for the underestimated simulated downward trend. Prior to 1978, two large SIC anomalies are simulated (1959 and 1969); these correspond to years with large ice exports through Fram Strait and a broad Transpolar Drift Stream causing lower SIC than normal (Tremblay et al. 1997). Since 1978, the observed sea level pressure has been decreasing in both the summer and winter months in the Arctic. A lower SLP results in a more divergent flow field for sea ice and typically more ice export. This can certainly account, in part, for the observed downward trend. When compared to the simulated SIC anomaly time series for all of the peripheral seas (Fig. 2), the East Siberian Sea appears to be the region most responsible for the negative trend in Arctic sea-ice extent, which is consistent with Arfeuille et al. (2000).

Fig. 7 Leading SVD mode of **a** the coupled sea-ice concentration (SIC) anomalies and **b** air temperature anomalies during 1958–97. The contour interval is 0.02 and the *darkened line* is the zero contour. The square covariance fraction corresponding to this mode is 57%. The *solid* and *dashed lines* in **c** represent the three-month-running mean of the time series of the expansion coefficients for the coupled SIC anomalies and air temperature anomalies respectively. The correlation coefficient between the expansion coefficients of both variables is 0.46 [0.13]

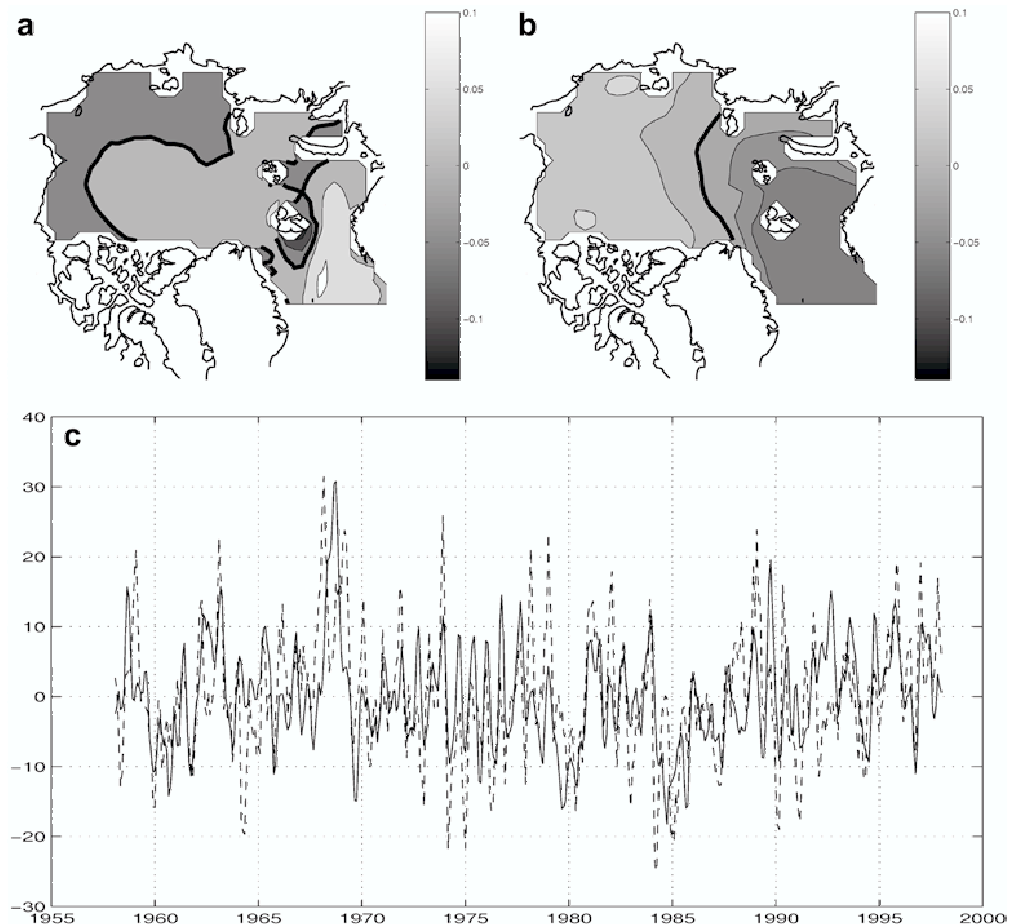
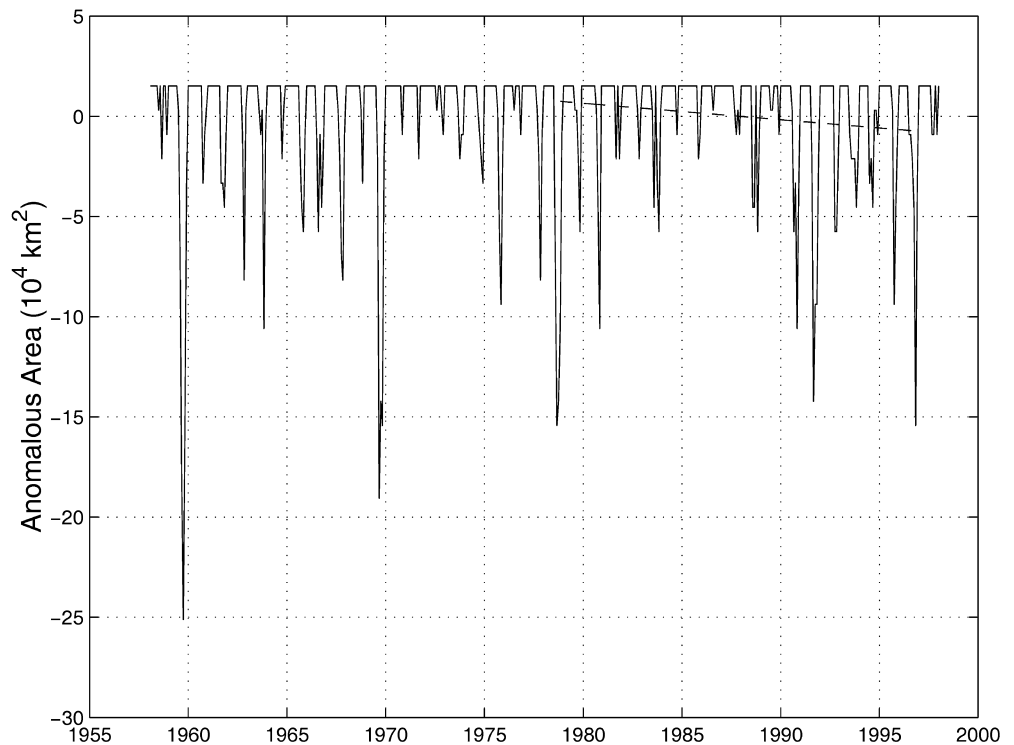


Fig. 8 Simulated monthly anomalies in sea-ice extent (*solid*) for 1958–1997, and the trend line for the November 1978 to December 1996 period superimposed (*dashed*). The downward trend is 1.1% per decade



5 Conclusions

Modelled Arctic sea-ice concentration (SIC) and corresponding observational data for the period 1958–97 have been compared to test the model's ability to simulate the observed SIC as well as to gain a better understanding of the thermodynamic and dynamic physical processes responsible for producing sea ice concentration anomalies. To help focus the discussion, several of the model-data intercomparisons were done on a regional basis.

In the regional study of area-averaged anomalous SIC time series, the model reproduces the observed variability reasonably well in the Beaufort, Chukchi, East Siberian and Laptev seas. The minima in SIC of the 1990s reported in recently published literature (Parkinson et al. 1999; Cavalieri et al. 1997; Maslanik et al. 1996; Serreze et al. 1995) are reproduced in the simulated results. The NCEP temperatures used to force the model are, in general, in good agreement with the EWG observed temperatures. In the Laptev Sea, however, for the winters 1980 and 1981, differences of peak winter temperatures were found to be ten degrees warmer than observed. Although this implies a significantly different surface energy budget, the model's sensitivity to thermodynamic forcing is lower than observed and so does not lead to a significant departure from the observed SIC. The model's sensitivity to southerly wind anomalies in producing SIC anomalies is in good agreement with the observed sensitivity. The analysis of river runoff data shows that it is not important in creating SIC anomalies in the total area of a

sea, although other studies show that it may have a local impact at the mouth of the river. The SVD analysis demonstrated that the main features of anomalous co-variability between SIC and ice speed in the Arctic were the contraction and expansion of the Arctic High and the strengthening and weakening of the ice velocities in the Transpolar Drift Stream. Finally, a downward trend over the past two decades of 1.1% per decade was calculated for the time series of the simulated extent of the Arctic sea-ice cover. This downward trend can mainly be attributed to negative anomalies in the East Siberian Sea.

Acknowledgements A. Armstrong is grateful to Dr. G. Holloway for useful discussions and suggestions, to S.A. Venegas for providing assistance with the statistical methods and to N. Rayner for providing valuable information concerning the HadISST data. A. Armstrong was supported in part by a student fellowship from the Centre for Climate and Global Change Research, which is funded by FCAR. B. Tremblay was supported by grant PF904713 from the International Arctic Research Centre (IARC) and grant OPP98-18711 from the National Science Foundation. This work was also supported by research grants awarded to L. Mysak from NSERC and the Canadian Institute for Climate Studies (Arctic Node). The NCEP Reanalysis data used in this study was provided by the NOAA-CIRES Climate Diagnostics Center, Boulder, Colorado, from their Web site at <http://www.cdc.noaa.gov/>.

References

- Atmospheric Environment Canada (1994) Water survey of Canada, Hydat CD-ROM, V.H.93, surface water and sediment data
- Arfeuille G, Mysak LA, Tremblay L-B (2000) Simulation of the interannual variability of the wind driven arctic sea-ice cover during 1958–1998. *Clim Dyn* 16: 107–121

- Barry RG, Serreze MC, Maslanik JA, Preller RH (1993) The arctic sea ice – climate system: observations and modeling. *Rev Geophys* 31: 397–422
- Becker T (1995) The effect of arctic river hydrological cycles on arctic ocean circulation. PhD Thesis. Old Dominion University, Virginia, USA
- Bitz CM, Fyfe J, Flato G (2002) Sea ice response to wind forcing from AMIP models. *J Clim* 15: 522–536
- Broecker WS, Denton GH (1990) The role of ocean–atmosphere reorganizations in glacial cycles. *Quat Sci Rev* 9: 305–341
- Cavalieri DJ, Glowersen P, Parkinson CL, Comiso JC, Zwally HJ (1997) Observed hemispheric asymmetry in global sea ice changes. *Science* 278: 1104–1106
- Chapman WL, Walsh JE (1993) Recent variations of sea-ice and air temperature in high latitudes. *Bull Am Meteorol Soc* 74: 33–47
- Chouinard LE, Garrigues L (1995) Interannual variability of the ice cover in the Chukchi and Beaufort seas. In: *Proc Fifth (1995) International Offshore and Polar Engineering Conference*, The Hague, The Netherlands. The International Society of Offshore and Polar Engineering, pp 357–363
- Coachman LK, Aagaard K (1988) Transports through Bering Strait – annual and interannual variability. *J Geophys Res* 93: 15,535–15,539
- Deser C, Walsh JE, Timlin MS (2000) Arctic sea ice variability in the context of recent atmospheric circulation trends. *J Clim* 13: 617–633
- Dickson RR, Osborn TJ, Hurrell JW, Meinke J, Blindheim J, Adlandsvik B, Vinje T, Alekseev G, Maslowski W (2000) The Arctic Ocean response to the North Atlantic Oscillation. *J Clim* 13: 2671–2696
- Flato GM, Brown RD (1996) Variability and climate sensitivity of landfast Arctic sea ice. *J Geophys Res* 101: 25,767–25,777
- Hibler III WD (1979) A dynamic thermodynamic sea ice model. *J Phys Oceanogr* 9: 815–846
- Levitus S (1994) World ocean atlas 1994, CD-ROM data sets
- Maslanik JA, Serreze MC, Barry RG (1996) Recent decreases in Arctic summer ice cover and linkages to atmospheric circulation anomalies. *Geophys Res Lett* 23: 1677–1680
- Mysak LA, Venegas SA (1998) Decadal climate oscillations in the Arctic: a new feedback loop for atmosphere-ice-ocean interactions. *Geophys Res Lett* 25: 3607–3610
- Newton R (2001) River runoff into the arctic ocean: results from a high-resolution ocean general circulation model and model-data comparisons. PhD Thesis. Lamont-Doherty Earth Observatory of Columbia University Palisades, NY, USA
- North GR, Bell TL, Cahalan RF, Moeng FJ (1982) Sampling errors in the estimation of empirical orthogonal functions. *Mon Weather Rev* 110: 699–706
- Oelke C (1996) The influence of the atmosphere on the remote sensing of sea ice using passive microwave radiometers. *Rep Polar Res* 1996 208: 1
- Parkinson CL, Cavalieri DJ, Gloersen P, Zwally HJ, Comiso JC (1999) Arctic sea ice extents, areas, and trends, 1978–1996. *J Geophys Res* 104: 20,837–20,856
- Prinsenberg SJ, Pererson IK, Narayanan S, Uj U (1997) Interaction between atmospheric ice cover and ocean off Labrador and Newfoundland from 1962–1992. *Can J Fish Aquat Sci* 54: 30–39
- Rayner NA, Parker DE, Horton EB, Folland CK, Alexander LV, Rowell DP (2002) Globally complete analyses of SST, sea ice and night marine air temperature, 1871–2000. *J Geophys Res* (in press)
- Roach AT, Aagaard K, Pease CH, Salo SA, Weingartner T, Pavlov V, Kinlakov V (1995) Direct measurements of transport and water properties through Bering Strait. *J Geophys Res* 100: 19,443–18,459
- Semtner AJ (1976) A model for the thermodynamic growth of sea ice in numerical investigations of climate. *J Phys Oceanogr* 6: 379–389
- Serreze MC, Maslanik JA, Key JR, Kokaly RF, Robinson DA (1995) Diagnosis of the record minimum in Arctic sea-ice during 1990 and associated snow cover extremes. *Geophys Res Lett* 22: 2183–2186
- Slonosky VC, Mysak LA, Derome J (1997) Linking Arctic sea-ice and atmospheric circulation anomalies on interannual and decadal time scales. *Atmosphere–Ocean* 35: 333–366
- Thompson DWJ, Wallace JM (1998) The Arctic Oscillation signature in the wintertime geopotential height and temperature fields. *Geophys Res Lett* 25: 1297–1300
- Tremblay LB, Mysak LA (1997) Modelling sea-ice as a granular material including the dilatancy effect. *J Phys Oceanogr* 27: 2342–2360
- Tremblay LB, Mysak LA (1998) On the origin and evolution of sea-ice anomalies in the Beaufort-Chukchi sea. *Clim Dyn* 14: 451–460
- Tremblay LB, Mysak LA, Dyke AS (1997) Evidence from driftwood records for century-to-millennial scale variations of the high latitude atmospheric circulation during the Holocene. *Geophys Res Lett* 24(16): 2027–2030
- Walsh JE (1978) A data set on northern hemisphere sea ice extent 1953–76. *Glaciological Data Report GD-2*, World Data Center-A for Glaciology (Snow and Ice): 49–51
- Walsh JE (1995) A sea ice database. In: Folland C, Rowell D (eds) *Workshop on simulations of the climate of the twentieth century using GISST*, 28–30 November 1994. Hadley Centre for Climate Prediction and Research CRTN 56, pp 54–58
- Yi D, Mysak LA, Venegas SA (1999) Decadal-to-interdecadal fluctuations of Arctic sea-ice cover and the atmospheric circulation during 1954–1994. *Atmosphere–Ocean* 37: 389–415
- Zhang J, Rothrock DA, Steele M (1998) Warming of the Arctic Ocean by a strengthened Atlantic inflow. *Geophys Res Lett* 25: 1745–1748